

Performance Analysis of Grid Connected PV/Wind Hybrid Power System during Variations of Environmental Conditions and Load

Omar Noureldeen*, Ahmed M. A. Ibrahim **‡

* Department of Electrical Engineering, Faculty of Engineering, South Valley University, Egypt

** Department of Electrical Engineering, Faculty of Engineering, South Valley University, Egypt

(A.Eldaker@eng.svu.edu.eg, omar_noureldeen@svu.edu.eg)

‡Corresponding Author; Ahmed M. A. Ibrahim, Egypt, Tel: +201098511516,

ahmedeldaker@hotmail.com

Received: 14.06.2017 Accepted: 25.07.2017

Abstract- This paper investigates a dynamic modeling, simulation and control of Photovoltaic (PV)-wind hybrid system connected to electrical grid and feeds large plant with critical variable loads. The technique of extracting maximum power point is applied for the hybrid power system to capture maximum power under varying climatic conditions. Moreover, Control strategy for power flow is proposed to supply critical load demand of plant. Modeling and simulation of the proposed hybrid system is performed using matlab-Simulink software. The Dynamic performance of the proposed hybrid system is analyzed under different environmental conditions. The simulation results have proven the effectiveness of the proposed maximum power point tracking (MPPT) strategies in response to rapid variations of weather conditions during the day. Moreover, the results show that when the injected power from hybrid system is larger than critical load power, the excess power will be injected to electrical grid. Otherwise, when injected power is lower than critical power demand, electrical utility grid in cooperated with hybrid power system will supply the critical load power. Moreover, when the injected power from hybrid system is unavailable, load demand is entirely fed by electrical utility.

Keywords PV, wind, hybrid system, MPPT control, DFIG, Load.

Nomenclature

$P_{station-A}$	Maximum power output from station (A)	$\lambda_{ds}, \lambda_{qs}$	Stator flux components in d-q axis
$P_{wind-farm}$	Maximum power from wind farm	V_{ds}, V_{qs}	Stator voltages components in d-q axis
$P_{station-B}$	Maximum power from station (B)	ω_e	Rotational speed of stator flux
P_{plant}	Power demanded by plant	i_{ds}, i_{qs}	Stator currents component in d-q axis
P_{Grid}	Injected power to/from electric grid	i_{dr}, i_{qr}	Rotor current components in d-q axis
I, V	Output current and voltage of PV array	L_m, L_s, L_r	Magnetising, stator inductance, rotor self-inductance.
I_{ph}, I_s	Light generated current and saturation current of PV	σ	Leakage factor

N_p, N_s	Number of parallel and series modules	R, L	Resistance, inductance of RL choke
R_s, R_{sh}	Series resistance and parallel resistance	P_{m_pu}	Mechanical power per unit
I_{sc}	Short circuit current at STC (Standard Test Condition)	q	Electron's charge
K_i	Short circuit temperature coefficient	A, K	Constant of Boltzmann and temperature of cell
E_g	Band gap energy of semiconductor used in cell	T, G	Temperature of cell and solar irradiance
I_{rs}	Reversed saturation current at T_{ref}	P, i_{or}	Number of poles and Rotor converter DC-link current
R_f, L_f	Resistance and inductance of filter	T_{ref}	Reference temperature (25°C)
P_{mech}	Mechanical power of wind turbine	V_{or}, ω_{ref}	Wind velocity and optimum rotational speed per unit
V_{dc}, C	DC link voltage and DC link capacitor	i_{ms}, m	Stator magnetizing current and Stator modulation factor
λ, β	Tip speed ratio and blade pitch angle	ρ, A_t	Air density and Area swept out by turbine blades
$V_{abc-conv}, I_{abc-conv}$	Voltage and current at DC/AC converter	V_{abc}, ω	Voltage at RL filter (grid voltage) and Grid frequency

1. Introduction

The permanent increase in the energy demand is considered as one of the most critical issue nowadays. Besides, as conventional power sources are limited and have adverse effects on the planet, has necessitated an imperative search for renewable energy which cause no pollution of the earth. Between these sustainable energy sources, wind and photovoltaic can be considered as the most promising technologies to produce electricity. Wind power can be utilized using large generators to generate great power capacity. Also, solar irradiation can be utilized as Photovoltaic power. Both photovoltaic and wind have their own demerits as they are intermittent in nature and immensely depend on the climate conditions, besides photovoltaic energy can be utilized only during daylight. Therefore, integration of these renewable energy resources as hybrid system can be used for overcoming intermittency and provide high reliability to maintain continuous output power to electrical grid or rural areas. Over recent years several investment and research have been investigated in PV/wind hybrid power system, such as Benadli [1-3], introduced sliding mode control for standalone PV/wind hybrid system. Oskouei [4], proposed quinary asymmetric inverter used in PV/wind hybrid power system with backup battery. Laabidi [5], presented modelling and control strategy of grid-connected PV/wind hybrid power system. Since, the extracted power from hybrid system is immensely dependent on the variations of environmental conditions such as solar irradiation and wind speed. Therefore, the maximum power point tracking (MPPT) strategies are essential to capture maximum power under varying climatic conditions. Several literatures deal with the MPPT control algorithms [1, 3, 6, 7], such as Abbassi [6], investigated fuzzy logic control for extracting maximum power from hybrid power system.

The doubly fed induction generator (DFIG) is the most commonly utilized in the wind energy conversion systems [8-10]. Several surveys have been carried out in PV and DFIG based-wind hybrid power system [11, 12]. Among them, Rajesh [11], presented PV and DFIG based-wind hybrid power system to supply continuous power for rural places. Kumar [12], proposed the connection of PV and DFIG based-wind hybrid power system with the electrical grid. Recently, more challenges on the grid-connected PV/wind hybrid power system occur. Among these challenges, enhancement of the injected power quality, extraction of maximum power, and the problems related to the connection of hybrid power system with the electrical grid under any conditions [13-15]. This study investigates detailed dynamic modeling, design and control of PV and wind as hybrid system interconnected to the electrical grid and supply large plant with critical variable loads. The proposed hybrid system consists of two Photovoltaic (PV) stations placed at different locations and one wind farm are integrated into main AC bus to enhance the system effectiveness. The technique of extracting maximum power point is applied for both photovoltaic stations and wind farm to capture maximum power under varying climatic conditions. The objective of this paper is to analyze hybrid system performance under various environmental conditions like variations of sun irradiance and wind speed. Moreover, power flow control method is proposed to supply critical load demand of large plant. The validation and effectiveness of the proposed power flow are evaluated under variation of the critical load demand.

2. The Proposed Hybrid Power System Model

Figure 1 depicts proposed hybrid power system. The proposed hybrid system consists of two Photovoltaic (PV) stations placed at different locations and one wind farm are integrated into main AC bus (25 kV-bus bar). Wind farm

equipped with Doubly Fed Induction Generator (DFIG). Also, the wind farm includes Rotor Side Converter (RSC) for extracting maximum wind power, and Grid Side Converter (GSC) to adjust DC bus voltage at specified value. PV stations (A, B) are subjected to different solar irradiations, where they are installed at different locations. The PV station is integrated into the Point of Common Coupling (PCC) bus through DC-DC converter and DC/AC converter. Incremental conductance MPPT technique is used for extracting maximum output power from PV array. PV/wind hybrid power system feeds a large plant with critical variable loads and the electrical utility grid. The plant is composed of 6 production lines. Each production line contains induction machine having rating of 2 MVA. When hybrid system injects power larger than plant demand (load), surplus power will be supplied to the electrical grid. Otherwise, when the injected power from hybrid system is lower than plant demand (load), electrical grid will feed load demand in cooperation with hybrid power system. In addition, when the injected power from hybrid system is unavailable, plant is entirely fed by electrical utility.

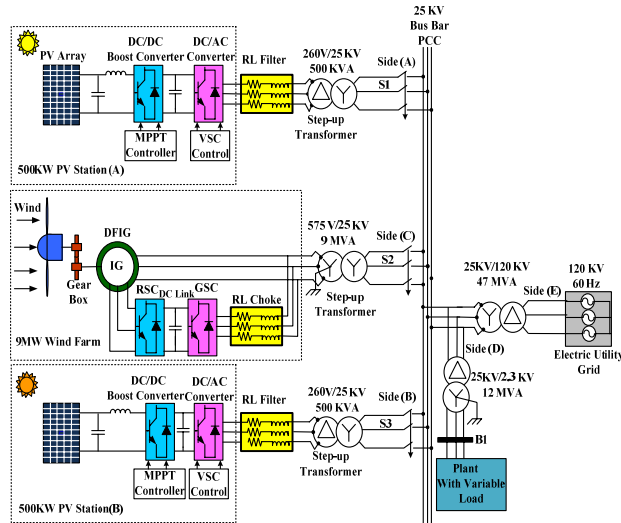


Fig. 1. Hybrid power system model.

3. Proposed Hybrid System Power Flow

3.1 Case 1- Injected Power from Hybrid System greater than Plant Load

In this case, the injected powers from PV stations and wind farm are greater than the load demand of the plant. Hence, the hybrid system injects power to the plant and electrical grid as follows:

$$P_{station-A} + P_{station-B} + P_{wind\ farm} = P_{Grid} + P_{plant} \quad (1)$$

3.2 Case 2- Injected Power from Hybrid System lower than Plant Load

In this case, the injected powers from PV stations and wind farm are smaller than the plant demand. Thus, the electrical grid will feed plant demand in cooperation with

hybrid power system. The hybrid system and electrical grid will inject power to the plant as follows:

$$P_{station-A} + P_{station-B} + P_{wind\ farm} + P_{Grid} = P_{plant} \quad (2)$$

3.3 Case 3- Injected Power from Hybrid System unavailable

When the injected power from hybrid System is unavailable, load demand of the plant is entirely fed by electrical utility as follows:

$$P_{Grid} = P_{plant} \quad (3)$$

The power flow of hybrid system can be summarized in Fig. 2.

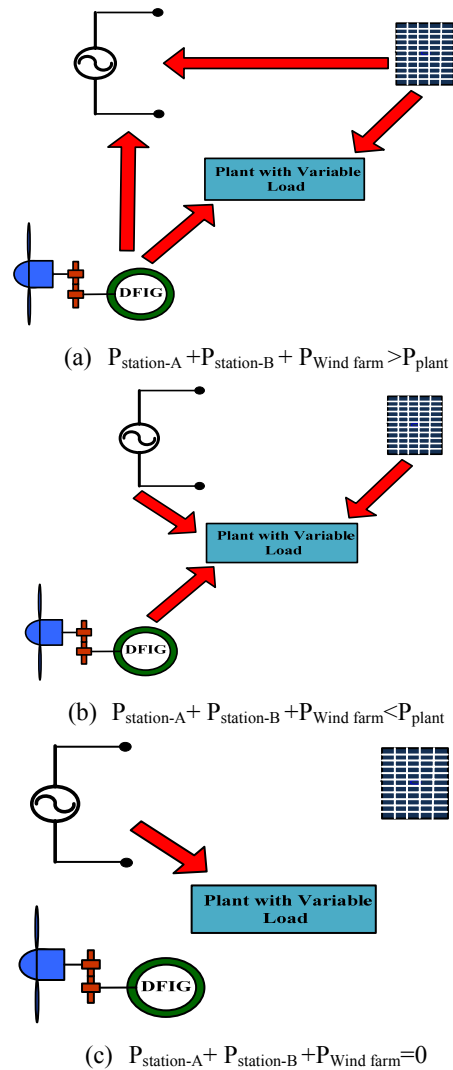


Fig. 2. Graphical representation of power flow.

4 Photovoltaic Conversion System

In this part, the electrical modelling of photovoltaic system and the characteristics of PV array are introduced. In addition, the MPPT technique and DC-AC inverter controller are discussed.

4.1 PV System Model

The modelling of photovoltaic system has been introduced based on the Shockley diode as shown in Fig.3 [8, 16]. The electrical characteristics of a PV array can be simulated with regard to the variations in the environmental conditions like sun irradiation intensity. The corresponding equation for current-voltage characteristics of PV array can be written as follows [1]:

$$I = N_p I_{ph} - N_p I_s \left\{ \exp \left[\frac{q \left(\frac{V + R_s I}{N_s N_p} \right)}{K T A} \right] - 1 \right\} - \left(\frac{N_p V + R_s I}{R_{sh}} \right) \quad (4)$$

$$I_{ph} = \frac{G}{1000} \cdot [I_{sc} + K_1(T - T_{ref})] \quad (5)$$

$$I_s = I_{rs} \cdot \left(\frac{T}{T_{ref}} \right)^3 \exp \left[\frac{q E_g}{K A} \cdot \left(\frac{1}{T_{ref}} - \frac{1}{T} \right) \right] \quad (6)$$

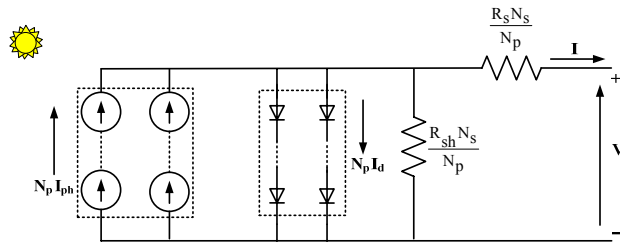
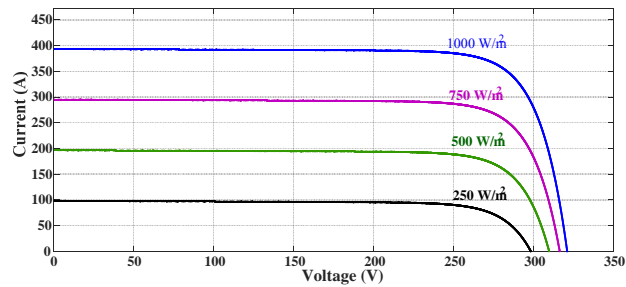
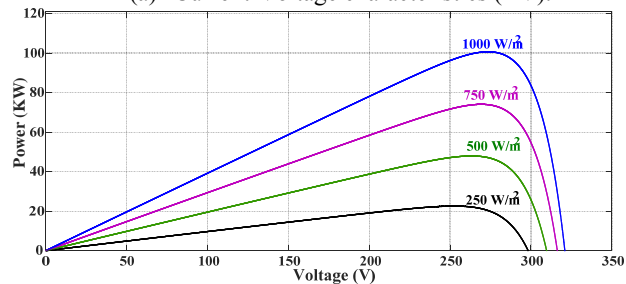


Fig. 3. PV array model.

Detailed specifications of each PV station are given in Appendix A. Fig.4 depicts current/voltage characteristics and power/voltage characteristics of each PV array under different solar irradiation intensity conditions.



(a) Current-Voltage characteristics (I-V).



(b) Power-Voltage characteristics (P-V).

Fig. 4. Characteristics of PV array.

4.2 Maximum Power Point Tracking Algorithm

Maximum power point tracking strategies are essential in the photovoltaic conversion systems. Since the intensity of solar irradiation varies with time, MPPT technique is used for extracting maximum output power from PV array. Previous surveys have introduced several MPPT [1, 6, 7, 17]. In this paper, incremental conductance MPPT algorithm is used due to advantage of offering good performance under rapid variation of solar irradiation [15, 18, 19]. Fig.5 depicts the corresponding flow chart of incremental conductance MPPT technique. The implementation of the MPPT technique in Simulink model is shown in Fig.6. The incremental conductance strategy is dependent on fact that the slope of Power-voltage (P-V) curve is equal to zero at the maximum power point (MPP). Also, the derivative of power with respect to voltage (dP_{pv}/dV_{pv}) is positive at left of the MPP, and negative at the right of the MPP. The mathematical model of this technique is as follows:

The output power of PV array

$$P_{pv} = V_{pv} * I_{pv} \quad (7)$$

$$\frac{dP_{pv}}{dV_{pv}} = \frac{d}{dV_{pv}} [V_{pv} * I_{pv}] = I_{pv} + V_{pv} \frac{dI_{pv}}{dV_{pv}} \quad (8)$$

Then,

$$\frac{dP_{pv}}{dV_{pv}} = 0, \quad \frac{dI_{pv}}{dV_{pv}} = -\frac{I_{pv}}{V_{pv}} \quad \text{at the MPP } \Delta V_n=0 \quad (9)$$

$$\frac{dI_{pv}}{dV_{pv}} > -\frac{I_{pv}}{V_{pv}} \quad \text{Left of the MPP, increment } V_{pv} \quad (10)$$

$$\frac{dI_{pv}}{dV_{pv}} < -\frac{I_{pv}}{V_{pv}} \quad \text{Right of the MPP, decrement } V_{pv} \quad (11)$$

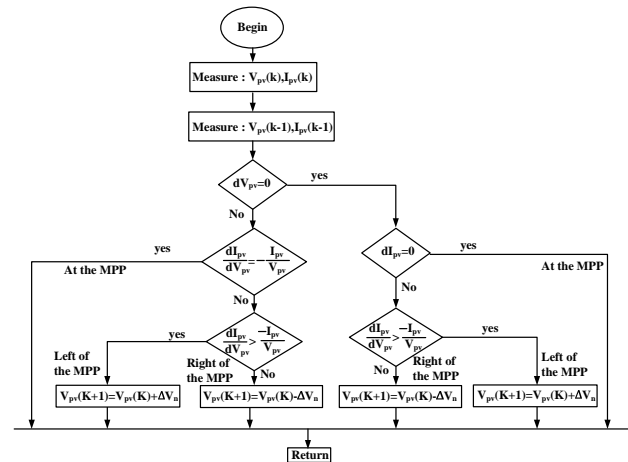


Fig. 5. Flow chart of incremental conductance technique.

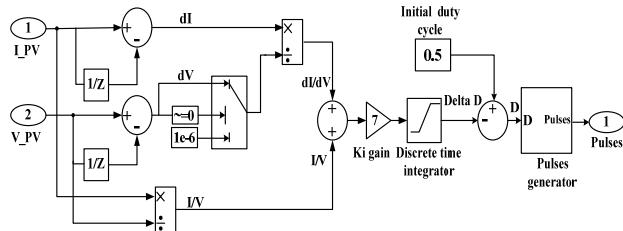


Fig. 6. Simulink model of PV MPPT control.

4.3 DC/AC Converter Controller

Figure 7 depicts control scheme of DC/AC converter controller. The main task of this controller is to regulate DC bus voltage, control injected active power to load and make unity power factor at PCC bus. This control strategy is beneficial for its decoupled control ability and fast dynamics [14, 15].

Then,

$$V_{abc} = V_{abc_conv} - R_f I_{abc_conv} - L_f \frac{dI_{abc_conv}}{dt} \quad (12)$$

Transforming Equation (12) into d-q rotating reference frame yield:

$$V_{d_conv} = R_f I_d + L_f \frac{dI_d}{dt} - \omega L_f I_q + V_d \quad (13)$$

$$V_{q_conv} = R_f I_q + L_f \frac{dI_q}{dt} + \omega L_f I_d + V_q \quad (14)$$

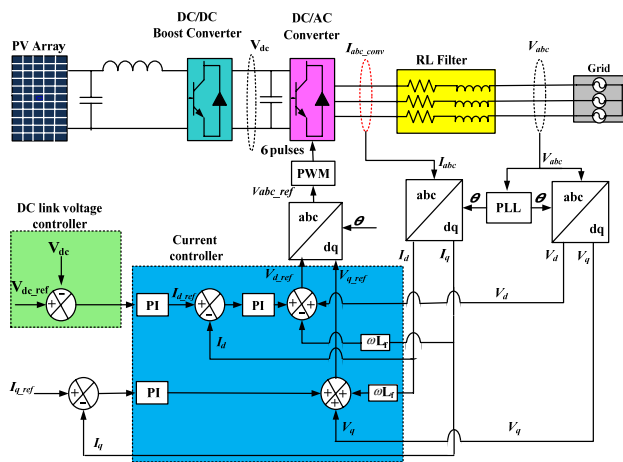


Fig. 7. DC/AC converter control scheme.

The phase locked loop is closed loop frequency control strategy. This structure estimates grid voltage angle (θ) for d-q coordinates and synchronize converter output voltage with the grid voltage and current [20]. Fig.8 displays the control scheme of the phase locked loop.

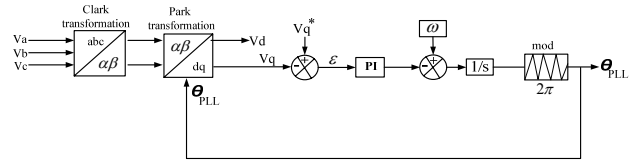


Fig. 8. Block diagram of phase locked loop.

4.3.1 DC Link Voltage Controller

The DC link voltage controller is responsible for regulating voltage at constant specified value. Reference voltage is compared with actual value and the difference is applied to PI-controller to regulate the voltage at 500V DC. The output of this controller is used as direct axis reference current (I_{d_ref}) for inner current controller.

4.3.2 Current Controller

The current controller loop control independently direct axis (I_d) and quadrature axis (I_q) of grid currents. The (I_{d_ref}) is derived from dc link voltage control while the (I_{q_ref}) is set to zero to maintain unity power factor. Aligning the direct-axis of grid voltage (V_d) with vector of grid voltage, quadrature-axis grid voltage (V_q) is set to zero. Thus, injected active power (P) and reactive power (Q) can be adjusted independently by I_d and I_q respectively [5]. Then,

$$P = \frac{3}{2} (V_q I_q + V_d I_d) = \frac{3}{2} V_d I_d \quad (15)$$

$$Q = \frac{3}{2} (V_q I_d - V_d I_q) = -\frac{3}{2} V_d I_q \quad (16)$$

5 Wind Energy Conversion System

In this section, the mechanical modelling of wind turbine and its characteristics are introduced. In addition, RSC controller, GSC controller, and MPPT technique are discussed.

5.1 Modeling of Wind Turbine

A wind turbine is modeled by an aerodynamic input torque which drives a doubly fed induction generator. Mechanical power (P_{mech}) extracted from wind turbine is described as follows [4]:

$$P_{mech} = \frac{1}{2} \rho A_t C_p (\lambda, \beta) V_\omega^3 \quad (17)$$

The power coefficient (C_p) represents the turbine efficiency and depends on the blade aerodynamics. Power coefficient (C_p) can be described as follows:

$$C_p (\lambda, \beta) = 0.5176 \left(\frac{116}{\lambda_i} - 0.4\beta - 5 \right) e^{\left(\frac{-21}{\lambda_i} \right)} + 0.0068\lambda \quad (18)$$

$$\frac{1}{\lambda_i} = \frac{1}{\lambda + 0.08\beta} - \frac{0.035}{\beta^3 + 1} \quad (19)$$

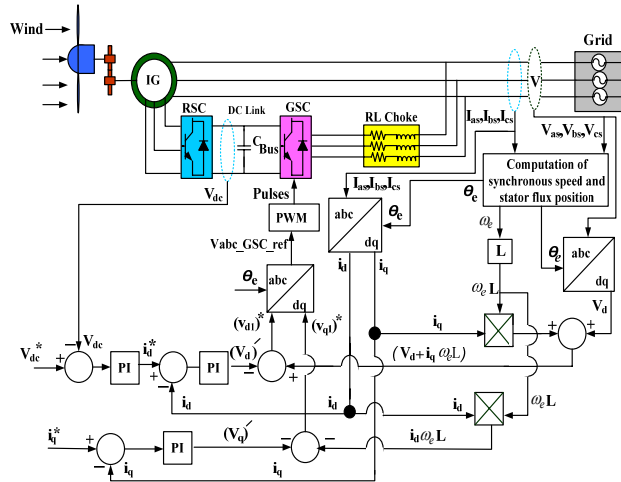


Fig. 11. Grid side converter controller.

5.4 Improved MPPT Control Strategy

The maximum power from wind turbine is extracted at optimum rotational speed of rotor (ω_{ref}). Thus, when the wind speed varies the MPPT controller calculates this optimum rotational speed to capture maximum power from wind turbine. Common MPPT techniques based on measurement of wind speed and wind turbine characteristics. Hence, the error in modeling of wind turbine and absence of accuracies in the sensors will affect the precision of the MPPT controller [23]. In this paper, an improved MPPT control technique has been proposed based on measurement of mechanical power (P_{m-pu}) to determine the optimum rotational speed (ω_{ref}). The flow chart of the MPPT controller is depicted in Fig.12. The MPPT control strategy can be explained as follows:

- Firstly, the controller set initial values for mechanical power (P_{m-pu}) and optimum rotational speed (ω_{ref}).
- Then, the controller calculates the actual mechanical power to calculate optimum rotational speed (ω_{ref}).
- If the mechanical power (P_{m-pu}) is greater than 0.75 p.u., the optimum rotational speed is normally 1.2 p.u. that corresponding to maximum power from wind farm (9 MW).
- If the mechanical power (P_{m-pu}) is lower than 0.75 p.u., the optimum rotational speed is calculated according to Eq. (29).

The improved MPPT control strategy can accurately calculate optimum rotational speed to track the maximum power without measurement of wind speed. The optimum rotational speed can be expressed as follows [23-25]:

$$\omega_{ref} = \begin{cases} 1.2 & 1 \geq P_{m-pu} \geq 0.75 \\ -0.67(P_{m-pu})^2 + 1.42(P_{m-pu}) + 0.51 & P_{m-pu} < 0.75 \end{cases} \quad (34)$$

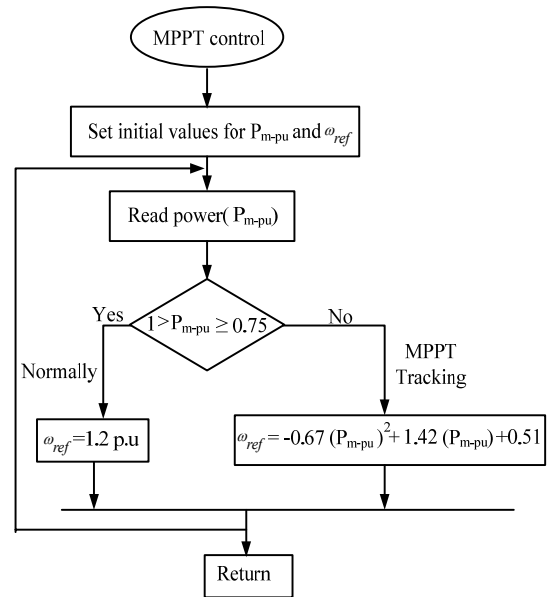


Fig. 12. Flow chart of the MPPT controller.

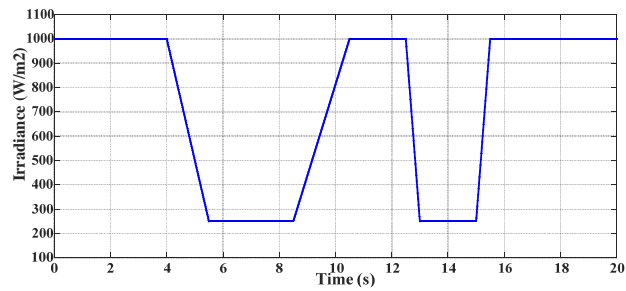
6 Simulation Results and Discussion

Detailed specifications of the PV-wind hybrid system depicted in Fig.1 are given in Appendix A. This section is divided into two parts: 1) performance of hybrid power system under different environmental circumstances like variations of sun irradiance and wind speed 2) validation of proposed power flow under variation of critical load demand of the plant. The simulation results indicate that proposed control strategies successfully achieved desired system performance. In addition, the proposed power flow control strategy successfully supplies the critical load demand of the plant.

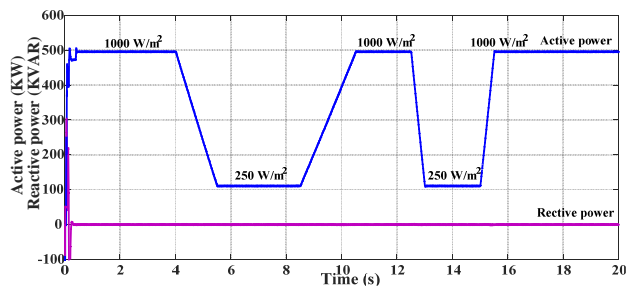
6.1 Performance of PV-Wind Hybrid Power System

6.1.1 Performance of PV Station (A)

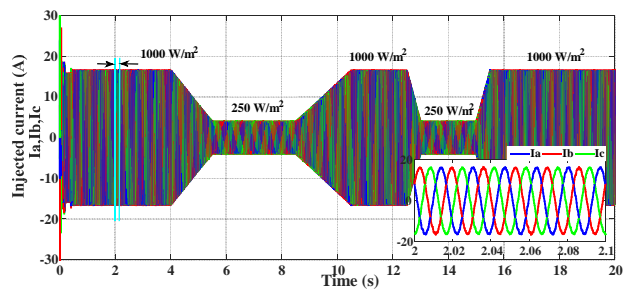
The performance of PV station (A) is analyzed under changes of solar irradiation as illustrated in Fig.13. PV array surface temperature is considered to be constant at 25°C during the complete simulation time. Fig.13 (a) depicts variation of sun irradiation [26]. This variation demonstrates the change of irradiation during a day and the shadow of cloud, for example. Fig.13 (b) shows that the injected active power from PV station (A) varies with its solar irradiance and the reactive power is zero therefore unity power factor. Fig.13 (c) displays the three-phase injected current. It can be noticed that the DC/AC converter controller regulates the amplitude of current as function of the injected power. Fig.13 (d) illustrates the effectiveness of system controller. Thus, Grid voltage is in phase with injected current due to unity power factor.



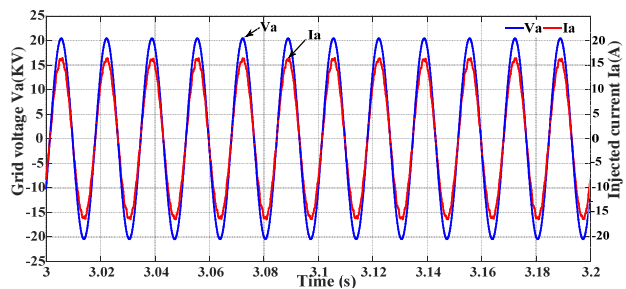
(a) Solar irradiance.



(b) Injected active power and reactive power.



(c) Injected current from PV station side (A).



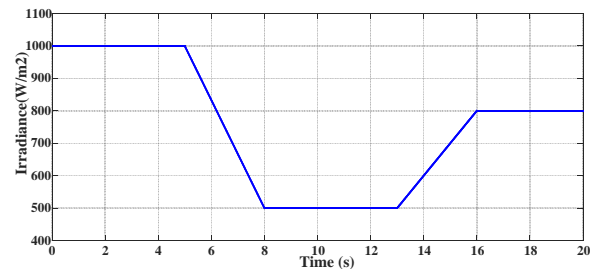
(d) Grid voltage and injected current.

Fig. 13. Performance of PV station (A).

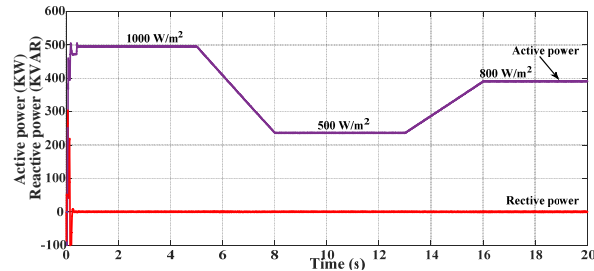
6.1.2 Performance of PV station (B)

The performance of PV station (B) is investigated under change of sun irradiation as depicted in Fig. 14. The change of sun irradiation is displayed in Fig. 14 (a) [27]. This change represents shadow of cloud, for example. Fig. 14 (b) shows that the injected active power from PV station (B) is very near to the generated value thus small losses and the injected reactive power is null therefore unity power factor. Fig. 14 (c) displays the three-phase injected current. The change of current amplitude reflects the variation of power since grid

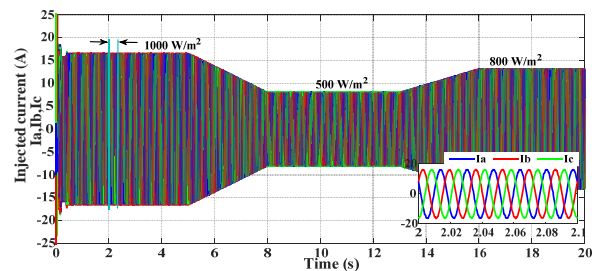
voltage remains constant. Fig. 14 (d) illustrates that the power factor of DC/AC converter is very close to one.



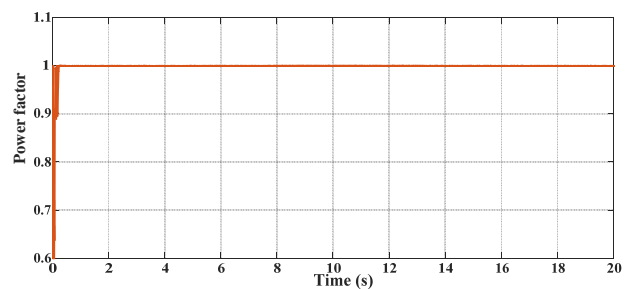
(a) Solar irradiance.



(b) Injected active power and reactive power.



(c) Injected current from PV station side (B).



(d) Power factor of DC/AC converter.

Fig. 14. Performance of PV station (B).

6.1.3 Performance of Wind Farm

Figure 15 shows the performance of DFIG wind farm under variation of wind speed. Speed variation for gradation wind is depicted in Fig. 15 (a) [28]. The ramp change of wind speed is in between 15 m/s and 10 m/s. Fig. 15 (b) shows that the injected active power from wind farm changes according to wind speed while delivered reactive power is maintained null thus unity power factor. Hence, the MPPT controller tracks accurately the optimum rotational speed when the wind speed varies continuously. Fig. 15 (c) displays the three-

phase injected current from wind farm. It can be noticed that the RSC controller regulates the amplitude of current as function of the injected power. It can be noticed from Fig.15 (d) that GSC controller maintain DC link voltage fixed at 1150 V regardless of magnitude of injected power.

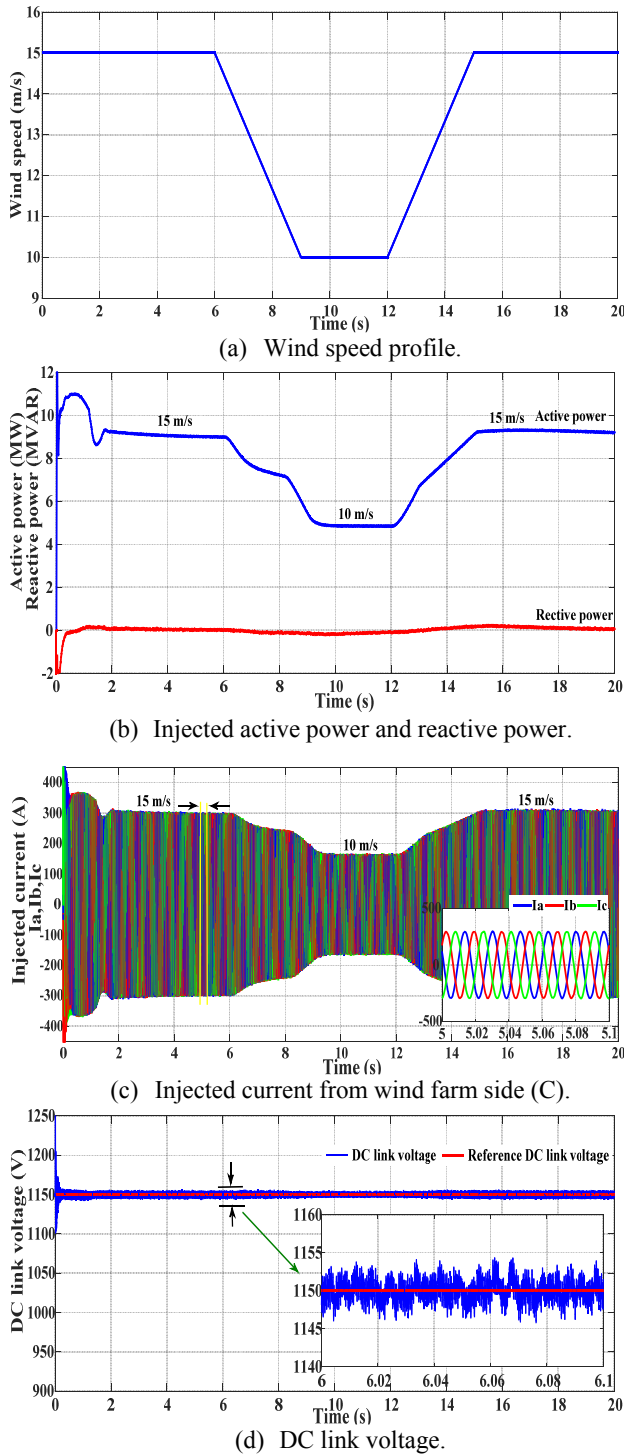


Fig. 15. Performance of wind farm

Figure 16 (a) depicts power balance of hybrid power system. It can be noted that injected power from hybrid system to the grid side (PCC-bus) is equal to sum of injected powers from PV station (A), PV station (B) and wind farm. Fig.16 (b) shows constant voltage of PCC-bus with peak value of 20 kV per phase (25 kV L-L). The PCC-bus voltage is constant irrespective of variations of injected power from hybrid system.

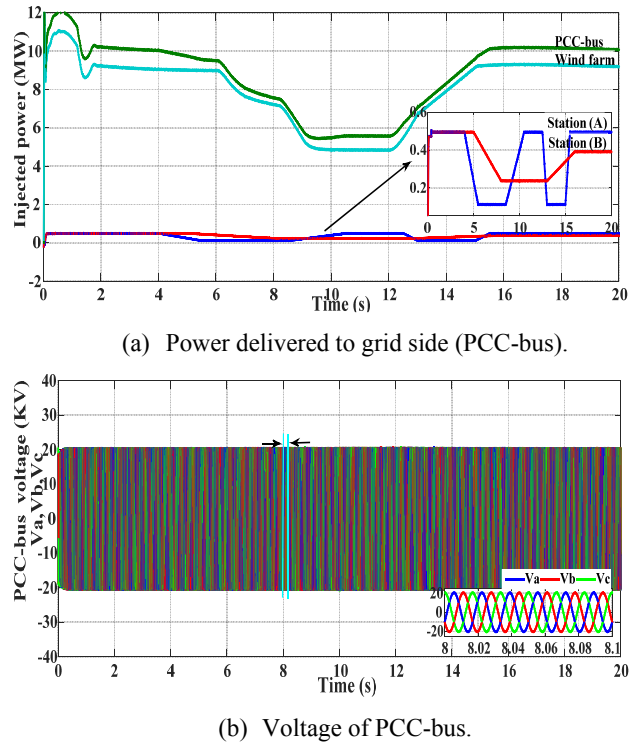
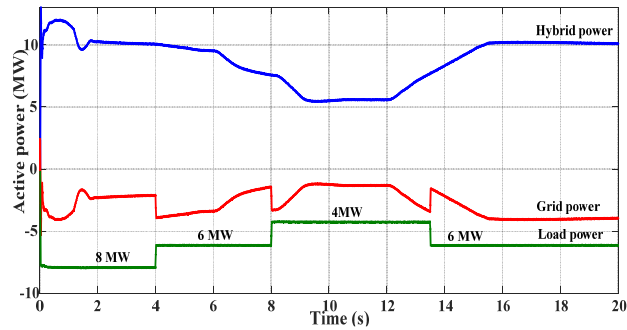


Fig. 16. Performance of PV-wind hybrid system at PCC-bus.

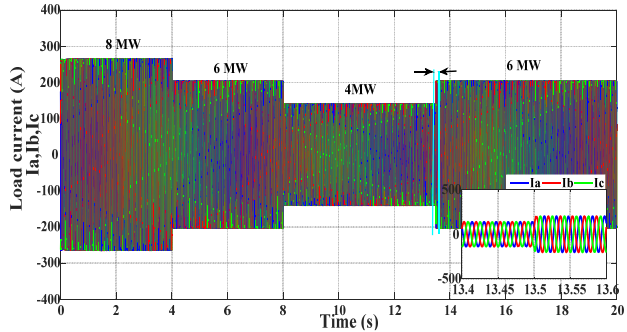
6.2 Validation of Proposed Power Flow

6.2.1 Injected Power from Hybrid System Larger than Plant Load

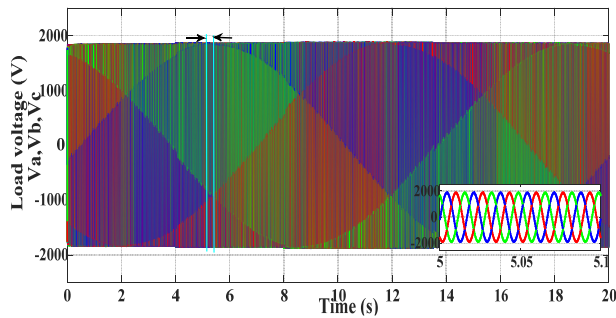
In this case, the generated powers from PV stations and wind farm are larger than critical load demanded power of plant. Therefore, the hybrid system will feed critical load of the plant and the surplus power will be injected to electrical grid as depicted in Fig.17 (a). Hence, according to Eq. (1) the hybrid system injects power to plant and electrical utility. Fig.17 (b) depicts the waveforms of three phase load current. The critical load demanded power is 8 MW with 262.3 A from 0 s to 4 s. During the duration from 4 s to 8 s the critical load power is decreased from 8 MW to 6 MW with 202.8 A. Then, the critical plant power is reduced to 4 MW with 139.3 A from 8 s to 13.5 s. Finally, the critical load power is suddenly returned to 6 MW. Fig.17 (c) shows constant load voltage regardless of variation of critical load power.



(a) power flow between hybrid system, grid and load.



(b) Load current side (D).

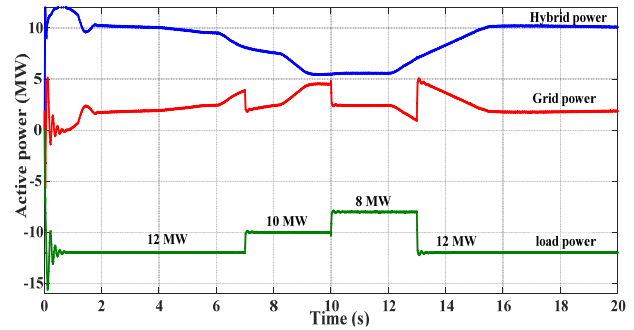


(c) Load voltage bus-B1.

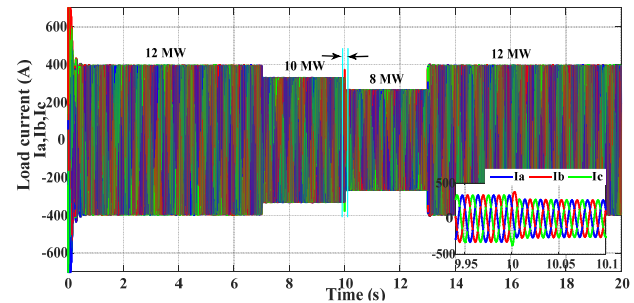
Fig. 17. Injected power from hybrid system greater than load demand for case 1.

6.2.2 Injected Power from Hybrid System Lower than Load Demand

In this case, injected power from hybrid system is smaller than critical demanded power of plant. Therefore, the electrical utility grid in cooperated with hybrid power system will feed critical demanded power of plant as depicted in Fig.18 (a). Thus, according to Eq. (2) the hybrid system and electrical grid will inject power to the plant load. Fig.18 (b) depicts the waveforms of three phase load current. The critical load demanded power is 12 MW with 392.2 A from 0 s to 7 s. During the duration from 7 s to 10 s critical demanded power is reduced from 12 MW to 10 MW with 325.9 A. Then, the critical demanded power is reduced to 8 MW with 262.3 A from 10 s to 13 s. Finally, the critical load power is suddenly returned to 12 MW.



(a) Real power flow between hybrid system, grid and load.



(b) Load current side (D).

Fig. 18. Injected power from hybrid system lower than load demand for case 2.

6.2.3 Injected Power from Hybrid System Equal to Zero

In this case, the hybrid System injects no power to the grid, so load demand of plant is entirely fed from electrical utility as depicted in Fig.19 according to Eq. (3).

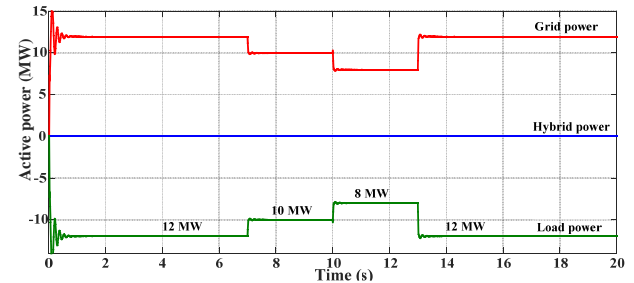


Fig. 19. Real power flow between hybrid system, grid and load when hybrid power is unavailable.

7 Conclusion

In this paper, modeling, simulation and control of grid connected photovoltaic-wind hybrid power system have been successfully investigated. The proposed hybrid system consists of two Photovoltaic (PV) stations placed at different locations and one wind farm are integrated into main AC bus and supply large plant with critical variable loads. The incremental conductance MPPT technique is applied for both

PV stations to extract maximum power under variations of solar irradiance. Also, an improved MPPT control strategy based on measurement of mechanical power is applied for wind farm to capture the maximum power under changes of wind speed. Moreover, control strategy for power flow is proposed to supply critical load demand of plant. The Dynamic performance of the proposed hybrid system is tested under different environmental conditions such as changes of solar irradiance and wind speed. In addition, the validation of the proposed power flow is evaluated under variation of the critical load demand. The simulation results have proven the robustness of the MPPT control strategies in response to rapid variations in weather conditions during the day. Moreover, the power flow control strategy successfully meets the critical load demand of the plant.

References

- [1] R. Benadli and A. Sellami, "Sliding mode control of a photovoltaic-wind hybrid system," in *Electrical Sciences and Technologies in Maghreb (CISTEM)*, 2014 International Conference on, 2014, pp. 1-8.
- [2] J. Hossain, N. Sakib, E. Hossain, and R. Bayindir, "Modelling and Simulation of Solar Plant and Storage System: A Step to Microgrid Technology," *International Journal of Renewable Energy Research (IJRER)*, vol. 7, pp. 723-737, 2017.
- [3] U. Choi, K. Lee, and F. Blaabjerg, "Power electronics for renewable energy systems: Wind turbine and photovoltaic systems," in *Renewable Energy Research and Applications (ICRERA)*, 2012 International Conference on, 2012, pp. 1-8.
- [4] A. B. Oskouei, M. R. Banaei, and M. Sabahi, "Hybrid PV/wind system with quinary asymmetric inverter without increasing DC-link number," *Ain Shams Engineering Journal*, vol. 7, pp. 579-592, 2016.
- [5] H. Laabidi and A. Mami, "Grid connected Wind-Photovoltaic hybrid system," in *Energy (IYCE)*, 2015 5th International Youth Conference on, 2015, pp. 1-8.
- [6] R. Abbassi, M. Hammami, and S. Chebbi, "Improvement of the integration of a grid-connected wind-photovoltaic hybrid system," in *Electrical Engineering and Software Applications (ICEESA)*, 2013 International Conference on, 2013, pp. 1-5.
- [7] R. Koad, A. F. Zobaa, and A. El Shahat, "A Novel MPPT Algorithm Based on Particle Swarm Optimisation for Photovoltaic Systems," *IEEE Transactions on Sustainable Energy*, 2016.
- [8] M. K. Hossain and M. H. Ali, "Transient stability augmentation of PV/DFIG/SG-based hybrid power system by parallel-resonance bridge fault current limiter," *Electric Power Systems Research*, vol. 130, pp. 89-102, 2016.
- [9] A. Parida and D. Chatterjee, "Cogeneration topology for wind energy conversion system using doubly-fed induction generator," *IET Power Electronics*, vol. 9, pp. 1406-1415, 2016.
- [10] B. Singh, S. K. Aggarwal, and T. C. Kandpal, "Performance of wind energy conversion system using a doubly fed induction generator for maximum power point tracking," in *Industry Applications Society Annual Meeting (IAS)*, 2010 IEEE, 2010, pp. 1-7.
- [11] K. Rajesh, A. Kulkarni, and T. Ananthapadmanabha, "Modeling and Simulation of Solar PV and DFIG Based Wind Hybrid System," *Procedia Technology*, vol. 21, pp. 667-675, 2015.
- [12] M. Kumar, K. Sandhu, and A. Kumar, "Simulation analysis and THD measurements of integrated PV and wind as hybrid system connected to grid," in *2014 IEEE 6th India International Conference on Power Electronics (IICPE)*, 2014, pp. 1-6.
- [13] T. R. Ayodele, A.-G. A. Jimoh, J. Munda, and J. Agee, "Dynamic Response of a Wind Farm Consisting of Doubly-Fed Induction Generators to Network Disturbance," in *Simulation and Modeling Methodologies, Technologies and Applications*, ed: Springer, 2013, pp. 131-150.
- [14] B. E. Strand, "Voltage Support in Distributed Generation by Power Electronics," 2008.
- [15] S. Gautam, D. B. Raut, P. Neupane, D. P. Ghale, and R. Dhakal, "Maximum power point tracker with solar prioritizer in photovoltaic application," in *Renewable Energy Research and Applications (ICRERA)*, 2016 IEEE International Conference on, 2016, pp. 1051-1054.
- [16] M. A.-E.-H. Mohamed, "Solar Irradiance Estimation of Photovoltaic Module based on Thevenin Equivalent Circuit Model," *International Journal of Renewable Energy Research (IJRER)*, vol. 5, pp. 971-972, 2015.
- [17] T. Miyagawa, H. Hayashiya, H. Yoshizumi, T. Furukawa, T. Iwakami, and A. Egami, "Examination of maximization of the photovoltaics electric power use by power distribution system control," in *Renewable Energy Research and Applications (ICRERA)*, 2012 International Conference on, 2012, pp. 1-5.
- [18] D. Sera, L. Mathe, T. Kerekes, S. V. Spataru, and R. Teodorescu, "On the perturb-and-observe and incremental conductance MPPT methods for PV systems," *IEEE journal of photovoltaics*, vol. 3, pp. 1070-1078, 2013.
- [19] S. Hesari, "Design and Implementation of Maximum Solar Power Tracking System Using Photovoltaic Panels," *INTERNATIONAL JOURNAL OF RENEWABLE ENERGY RESEARCH*, vol. 6, pp. 1221-1226, 2016.
- [20] A. Althobaiti, M. Armstrong, and M. Elgendy, "Current control of three-phase grid-connected PV inverters using adaptive PR controller," in *Renewable Energy Congress (IREC)*, 2016 7th International, 2016, pp. 1-6.
- [21] E. Aydin, A. Polat, and L. Ergene, "Vector control of DFIG in wind power applications," in *Renewable Energy Research and Applications (ICRERA)*, 2016 IEEE International Conference on, 2016, pp. 478-483.

- [22] A. Parida and D. Chatterjee, "Model-based loss minimisation scheme for wind solar hybrid generation system using (grid-connected) doubly fed induction generator," IET Electric Power Applications, vol. 10, pp. 548-559, 2016.
- [23] M. Zhou, G. Bao, and Y. Gong, "Maximum power point tracking strategy for direct driven PMSG," in Power and Energy Engineering Conference (APPEEC), 2011 Asia-Pacific, 2011, pp. 1-4.
- [24] N. W. Miller, W. W. Price, and J. J. Sanchez-Gasca, "Dynamic modeling of GE 1.5 and 3.6 wind turbine-generators," GE-Power systems energy consulting, 2003.
- [25] V. Rajasekaran, "Modeling, simulation and development of supervision control system for hybrid wind diesel system," 2013.
- [26] T. Haripriya, A. M. Parimi, and U. Rao, "Performance evaluation of DC grid connected solar PV system for hybrid control of DC-DC boost converter," in Intelligent Systems and Control (ISCO), 2016 10th International Conference on, 2016, pp. 1-6.
- [27] A. Cupertino, J. De Resende, H. Pereira, and S. S. Júnior, "A grid-connected photovoltaic system with a maximum power point tracker using passivity-based control applied in a boost converter," in Industry Applications (INDUSCON), 2012 10th IEEE/IAS International Conference on, 2012, pp. 1-8.
- [28] G. S. Kaloi, J. Wang, and M. H. Baloch, "Active and reactive power control of the doubly fed induction generator based on wind energy conversion system," Energy Reports, vol. 2, pp. 194-200, 2016.

Appendix A

Table A.1 Detailed specifications of DFIG

Element	Parameter
Rotor type	Wound rotor
Rated power	6*1.5=9 MW
Stator nominal voltage	575 V (L-L)
Nominal frequency	60 Hz
Stator resistance	0.023 pu
Stator inductance	0.18 pu
Rotor resistance	0.016 pu
Rotor inductance	0.16 pu
Magnetizing inductance	2.9 pu
Pairs of poles	3
Nominal DC link voltage	1150V

Table A.2 Detailed specifications of solar PV station

Element	Parameter
STC	T _{stc} =25°C, G _{stc} =1000 W/m ²
Number of arrays per station	5
Number of parallel strings	96
Number of series modules per string	5
Module type	Sun power SPR-305-WHT
Maximum power per array(P _{mpp})	100.7 KW
Voltage at MPP(V _{mpp})	273.5 V
Current at MPP (I _{mpp})	386.3 A
Open circuit Voltage (V _{oc})	321 V
Short circuit current (I _{sc})	393.4 A
Power factor of DC/AC converter	unity

Table A.3 Detailed specifications of wind turbine

Element	Parameter
Base wind speed	15 m/s
Maximum power at base wind speed	1.5 MW
Base Rotational speed	1.2 pu
Nominal performance coefficient	C _P =0.48 p.u
Coefficient(c ₁ -c ₆)	[0.5176,116,0.4,5,21,0.0068]

Table A.4 Detailed specifications of Plant

Element	Parameter
Number of induction machines	6 motors
Rotor type	Squirrel-cage
Rated apparent power/motor	2 MVA
Nominal voltage	2300 V (L-L)
Nominal frequency	60 Hz
Power factor	0.93

Table A.5 Specifications of transmission line and grid

Element	Parameter
Length of T.L	10 km
Grid voltage	120 kV(L-L)
Frequency	60 Hz